OPEN ACCESS
IOP Publishing | International Atomic Energy Agency
Nuclear Fusion
Nucl. Fusion **58** (2018) 126024 (9pp)
https://doi.org/10.1088/1741-4326/aae39a

Study of MHD mode and cooling process during disruptions triggered by impurities injection in J-TEXT

Y. Huang[1], Z.Y. Chen[1,2,a], Qiming Hu[1,a,b], Q. Yu[3], Z.H. Jiang[1], Y.N. Wei[1], Pengjuan Su[1], Chengshuo Shen[1], Daojing Guo[1], Z.J. Yang[1], X.M. Pan[1], Mingxiang Huang[1], Qinxue Cai[1], Tong Wang[1], Z.F. Lin[1], R.H. Tong[1], W. Yan[1], Z.P. Chen[1], Y.H. Ding[1], Y. Liang[1] and J-TEXT Team[1]

[1] International Joint Research Laboratory of Magnetic Confinement Fusion and Plasma Physics, State Key Laboratory of Advanced Electromagnetic Engineering and Technology, School of Electrical and Electronic Engineering, Huazhong University of Science and Technology, Wuhan 430074, People's Republic of China
[2] Chengdu University, 610106 Chengdu, People's Republic of China
[3] Max-Planck-Institut für Plasmaphysik, 85748 Garching, Germany

E-mail: zychen@hust.edu.cn and qhu@pppl.gov

Received 17 June 2018, revised 18 September 2018
Accepted for publication 24 September 2018
Published 11 October 2018

Abstract

The injection of a large amount of impurities is one of the possible ways of mitigating disruption in large-scale tokamaks. The deposition of impurities at the center of the plasma is the key to the radiation of plasma energy and suppression of runaway. The interaction of the gas jet with the rational surfaces has been studied by scanning the plasma current. The experimental results show that the injection of a massive amount of argon can cool the plasma from the edge to the core region, and the cooling process is accompanied by different magnetohydrodynamic (MHD) modes when the gas jet reaches the corresponding rational surfaces. It is observed that with different edge safety factors and electron density, gas injection can induce different poloidal modes at first. Then, the poloidal mode traverses to lower m (where m is the poloidal mode number) MHD activities until a 2/1 mode is initiated and a thermal quench is started. The experimental results show that the penetration of a gas jet across the rational surfaces is faster in the plasmas with pre-existing large 2/1 tearing modes, which indicates that the 2/1 mode plays an important role in the penetration process. Disruptions triggered by supersonic molecular beam injection display a slower cooling process compared with massive gas injection, which can be divided into four stages. The dominant poloidal mode transition from $m = 3$ to $m = 2$ is associated with electron temperature recovery.

Keywords: disruption, massive gas injection, magnetic perturbation, tokamak

(Some figures may appear in colour only in the online journal)

[a] Author to whom any correspondence should be addressed.
[b] Current address: Princeton Plasma Physics Laboratory, Princeton, NJ 08543-0451, United States of America.

Original content from this work may be used under the terms of the Creative Commons Attribution 3.0 licence. Any further distribution of this work must maintain attribution to the author(s) and the title of the work, journal citation and DOI.

1. Introduction

Plasma disruption in a tokamak is the sudden loss of magnetic confinement, i.e. a rapid, complete loss of plasma thermal and magnetic energy [1–3]. A disruption mitigation system is required in fusion reactors, since a disruption in a large device can cause serious damage [4]. Massive gas injection (MGI), a disruption mitigation method, is used to reduce electromagnetic forces, radiate the plasma energy,and suppress the generation of runaway electrons. Most MGI experiments have one or more fast-opening valves that deliver a massive amount of gas into plasmas. MGI has been successfully used as a rapid shutdown method in tokamaks [4].

Plasma performance after MGI is quite complex [5–11]. After the valve opens and the gas reaches the plasma edge, impurities diffuse into plasma, magnetohydrodynamic (MHD) activities are destabilized, growing tearing modes lead to a thermal quench (TQ) and the beginning of a current quench [12]. Recent research has shown that the 2/1 mode plays an important role in plasma cooling and impurity mixing with the hot plasma [12, 13]. There may be also other islands such as $m/n = 5/3$ and $m/n = 3/2$ islands existing before a major disruption [14] (where m and n are the poloidal and toroidal mode numbers, respectively).

Both numerical simulation and experiments have shown that the species of impurities, the working pressure of the MGI valve, and the q-profile have an important impact on the efficiency of disruption mitigation. Impurity mixing and radiation change the MHD activity and vice versa [3, 5, 13, 15]. Numerical investigation for C-Mod has shown that a TQ is triggered even at very shallow penetration [16]. Simulations for DIII-D plasmas reveal that the phase relationship between the tearing mode and the impurity location can affect both radiation peaking factor and impurity mixing, and it also suggested that a 1/1 mode can result in asymmetrically radiated power [17]. Simulation with JOREK shows that in MGI triggered disruption, the O-point of the magnetic island excited by MGI is located at the gas deposition position. The MGI causes the growth of a magnetic island ($m/n = 2/1$ and 3/2 mainly) and an 1/1 internal kink mode [18]. The 3/2 island grows when a 2/1 island gets larger, since the 2/1 tearing mode steeps the current profile inside the $q = 3/2$ surface [18, 19].

For understanding the process of impurity penetration, extensive experiments have been carried out on the Joint Texas Experimental Tokamak (J-TEXT) tokamak to scan the amount of gas injection, edge safety factor, and line-average electron density. It was observed that different MHD modes were destabilized with different experimental parameters. The experimental results are given in section 2. Finally, a summary is presented in section 3.

2. Experimental results on the penetration of gas jet

2.1. Experimental setup

J-TEXT is the former TEXT tokamak (that operated at the University of Texas at Austin in the 1980s) reconstructed and renamed in Wuhan [20]. It is a conventional iron core and circular cross-section tokamak with a major radius of $R_0 = 1.05$ m and a minor radius of $r = 0.25$–0.27 m with a movable limiter [21]. The maximum toroidal magnetic field is $B_T = 2.5$ T. The maximum plasma current is $I_P = 240$ kA with a 600 ms pulse length. The line average electron density is in the range of $n_e = (0.5–7) \times 10^{19}$ m^{-3} and an electron temperature of $T_e \sim 1$ keV [22].

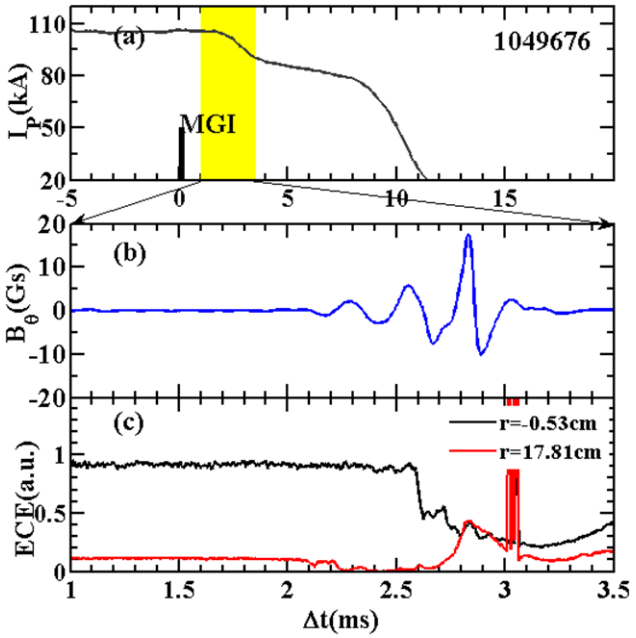

Figure 1. Time evolution of the (*a*) plasma current, (*b*) poloidal magnetic perturbation, and (*c*) ECE signals at two different radial locations for shot 1049676. The red spikes in (*c*) are invalid because the optical thickness condition for ECE measurement is not satisfied. The shadowed area in (*a*) is described in detail in (*b*) and (*c*). The times on the figure refer to the beginning time of MGI.

There are two poloidal arrays of 2D Mirnov coils and one array of 24 coils (arranged in a circular shape) for the detection of MHD activities [20, 23]. The electron cyclotron emission (ECE) diagnostic system consists of a 16-channel heterodyne ECE detecting unit and a new 8-channel W-band detecting unit, which covers a large portion of the plasma and has a temporal resolution of 2 μs and a spatial resolution of less than 1.5 cm [24, 25]. The fast framing camera, which has 22 k frame rate with 604 × 480 pixel resolution, has been developed to observe the penetration of an impurity gas jet on J-TEXT [26].

Two MGI valves have been developed for the J-TEXT tokamak. A 30 ml MGI valve is installed at the bottom port. It works in the range of 5–30 bar and the reaction time is about 0.3 ms [27]. As soon as the MGI valve opens, high-pressure gas can be injected into the plasma at sound speed. A supersonic molecular beam injection (SMBI) system has also been developed in the J-TEXT tokamak. The number of particles in the SMBI is linearly proportional to the product of gas pressure and pulse duration [28]. The SMBI system can inject lower amounts of particles than the MGI does. Becasue the large scale of argon injected into plasma will trigger a very fast cooling process in less than 1 ms, it is very difficult to

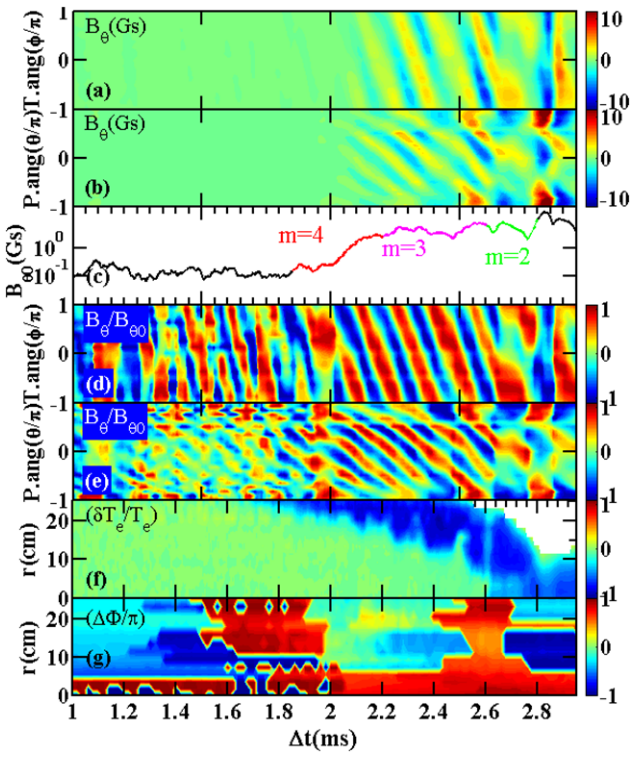

Figure 2. (*a*) Poloidal magnetic perturbation from toroidal Mirnov array, (*b*) poloidal magnetic perturbation from poloidal Mirnov array, and (*c*) maximum value of poloidal magnetic perturbation. Red, magenta, and green lines in frame (*c*) correspond to times when the poloidal mode number equals 4, 3, and 2, respectively. (*d*) Normalized poloidal magnetic perturbation from toroidal Mirnov array, (*e*) normalized poloidal magnetic perturbation from poloidal Mirnov array, and (*f*) time evolution of electron temperature at different minor radii for shot 1049676. T_e at different positions is the average value measured from each channel of the ECE from $\Delta t = -0.1$ ms to $\Delta t = 0$ ms, and δT_e is the instantaneous temperature variation with respect to T_e. $\delta T_e/T_e$ describes the relative change in electron temperature. The times on the figure refer to the beginning time of MGI. The white area in (*f*) after 2.4 ms is invalid because the optical thickness condition for ECE measurement is not satisfied. Figure (*g*) is the phase difference between ECE signals and one channel Mirnov signal.

diagnose any useful signal. Moderate injection of argon atoms was chosen to slow down the cooling process to make measurement feasible.

2.2. Time evolution of plasma performance after argon MGI

A typical result of MHD triggered by MGI is displayed in figure 1. The plasma parameters of discharge #1049676 are: plasma current $I_P = 105$ kA, toroidal field $B_T = 2.14$ T, edge safety factor $q_a = 6.3$, and the central line-average electron density $n_e \sim 1.5 \times 10^{19}$ m^{-3}. The MGI is triggered at 0.4 s. The injected argon atoms are about 2.6×10^{19}. The argon gas cooled down the plasma core with about a 3 ms delay. The injection of argon initiates a magnetic perturbation within ~2 ms after MGI is triggered. There are some oscillations of the ECE signal at $r = -0.53$ cm (high field side), which show that the cooling process is nonlinear. The signal of the plasma current shows that there is a runaway current plateau lasting about 6 ms. The analysis of the Mirnov coil array and the ECE diagnostic system in figure 2 shows the detailed evolution of the MHD activities and cooling process of this discharge after the MGI is triggered. Since the amplitude of the magnetic perturbation is small in the beginning, we chose a normalized amplitude to study the MHD activities.

Figures 2(*a*) and (*b*) show that after gas injection, the magnetic perturbation grows a short time later. Before MGI triggering, the amplitude of magnetic perturbation is tiny and no big island is presented in the plasma. Magnetic perturbations triggered by the impurity injection grow nonlinearly as the cooling front enters plasma as can seen from figure 2(*c*). Figures 2(*d*) and (*f*) show that the first MHD mode induced by massive argon is a $m/n = 4/1$ mode. With deeper plasma cooling, $m/n = 3/1$ and $m/n = 2/1$ modes appear in succession, which suggest impurity deposition at the corresponding rational surfaces. The ECE diagnostic system, which covers almost the entire low field side at $B_T = 2.14$ T, shows that plasma cooling has two processes: diffusive cooling and oscillating cooling.

The massive injected gas cools down the plasma from edge toward the central region as time involves, resulting in plasma current shrinkage and peaking [19]. This can temporally lead to a larger plasma current density gradient inside a resonant surface with $q = m/n$ but a smaller one outside the surface, and the (m, n) tearing mode can be destabilized. In addition, the shrinking current leads to the decrease of the effective edge q, the q value at the edge of the plasma current channel [29]. An external kink-type mode might be destabilized when the effective edge q decreases a little lower than m/n [22, 29]. The phase difference between ECE signals and one channel Mirnov signal plotted in figure 2(*g*), obtained by correlation analysis, shows that the $m = 4$ MHD activity is a kink-type mode or an island to small to be measured. While the later $m = 3$ and 2 activities are tearing modes according to the phase inversion, and these tearing modes cause observable temperature perturbations, namely, oscillating cooling. The high-m modes ($m = 6$, 5, and 4) usually grow only to low amplitude and survive only for a short period of time, and this stage behaves as a diffusive cooling process. At the end of the cooling process, the measurement of $\delta T_e/T_e$ in the white area is invalid because the optical thickness condition for ECE measurement is not satisfied.

Figure 3 shows four photos during the penetration of the gas jet before TQ onset. When the injection of argon atoms reached the plasma boundary, strong emissions were observed by a fast frame camera with a band-pass filter of a central wavelength of 442.6 nm. From the fast camera picture sequence, it is clear that the impurities spread preferentially toward the high-field side. Just before the TQ (~2.8 ms after MGI triggering), the dark area shows that the impurities have not totally spread into the plasma at this time.

To find the dependence of MHD activity (triggered by MGI) on the edge safety factor q_a, four discharges with different q_a are presented in figure 4. The plasma current of these four shots in figure 4 are: (*a*) 104 kA, (*b*) 120 kA, (*c*) 151 kA, and (*d*) 195 kA, respectively. The corresponding edge safety factors are about: (*a*) 6.3, (*b*) 5.5, (*c*) 4.5, and (*d*) 3.4, respectively. The line-average electron density is about 1.7×10^{19} m^{-3}

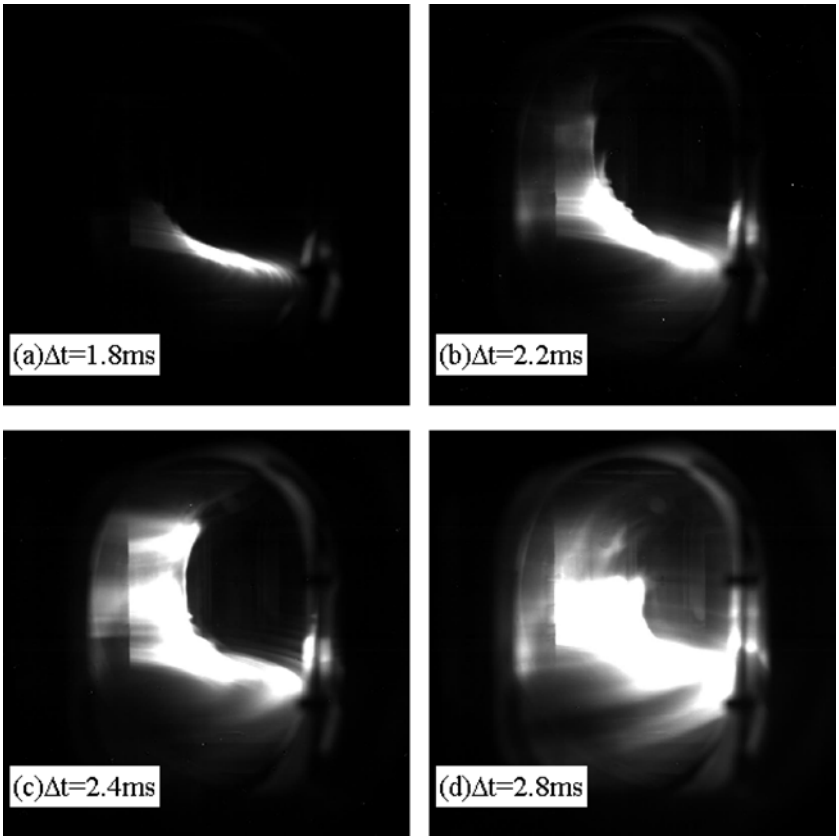

Figure 3. Observation of the penetration of the gas jet followed by disruption by a fast frame camera with a filter for shot 1049676. The times on the images refer to the beginning time of MGI. (a), (b), (c) and (d) show the time evolution of argon gas jet. Each image's left side is the high-field side. At $\Delta t = 2.8$ ms the core of plasma is cooled.

in these shots. The number of argon atoms injected in each shot is about 2.1×10^{19}. Figures 4(a1)–(d1) show almost the same increase in the magnetic perturbation. With different edge safety factors, the MGI initially triggers a different MHD mode. As the edge safety factor decreases, the poloidal number of the first MHD activity decreases as well. The MHD modes around the outermost rational surface are not visible in the figure, perhaps because they are too weak to be distinguished with Mirnov coils. The time delay between impurity reaching the edge and the collapse of the core electron temperature is very similar in these shots. If $q_a \sim 3$, the 2/1 island appears first, and cooling from the $r \sim 15$ cm to $r \sim 0$ cm occurs simultaneously. The spatial resolution of ECE is about 1.8 cm in these experiments, and we did not observe the temperature flattening from neighboring 3 channels, so that the 2/1 island width should be around 1.8–3.6 cm or smaller. This indicates that the 2/1 mode has an important influence on plasma cooling.

The effect of electron density on the MHD activities induced by MGI has also been studied. Two discharges were carried out with different electron density, while about 2.1×10^{19} argon atoms were injected through the MGI valve at 0.4 s. Figure 5 shows that the electron density before the MGI has an impact on induced MHD activities. The discharge with lower electron density (shot 1048977) has a higher poloidal mode number after the MGI. In figure 5(b2), for shot 1048998 with a higher density, the MHD mode resulting from the MGI is a 2/1 tearing mode, it grows very quickly compared to that in shot 1048977 shown by figure 5(a2). The cooling processes are quite different in these two shots. Cooling from the edge to core in shot 1048998 is much faster than that in shot 1048977, and this can be attributed to the onset of the $m/n = 2/1$ MHD mode at the beginning. It is worth mentioning that the 2/1 mode triggered by MGI at high electron density in figure 5(b1) has the fastest growth rate, even faster than that at the lower q_a discharge shown in figure 4(d1). For Ohmic discharges, the injected impurity due to MGI increases plasma radiation and may cause a radiation limit [30–32]. As a result, MGI may lower the Greenwald density limit and accelerate the excitation of precursor MHD, so that the 2/1 mode is excited earlier and grows faster.

Figures 6 and 7 show the relationship of MHD modes triggered by MGI with edge safety factor, electron density and amounts of injected argon atoms. Due to the fact that the toroidal mode number equals 1 in all cases, only poloidal mode numbers are presented. It can be seen that the value of m may get close to the value of the safety factor of the outer most rational surface when the central line-averaged electron density is about 1×10^{19} m^{-3}. The electron temperature is lower in higher electron density Ohmic discharges on J-TEXT [33]. In this case the injected gas will cause a relatively smaller further decrease in electron temperature compared to that in low density discharges. The corresponding relative change in the plasma current density profile is also smaller. This might be

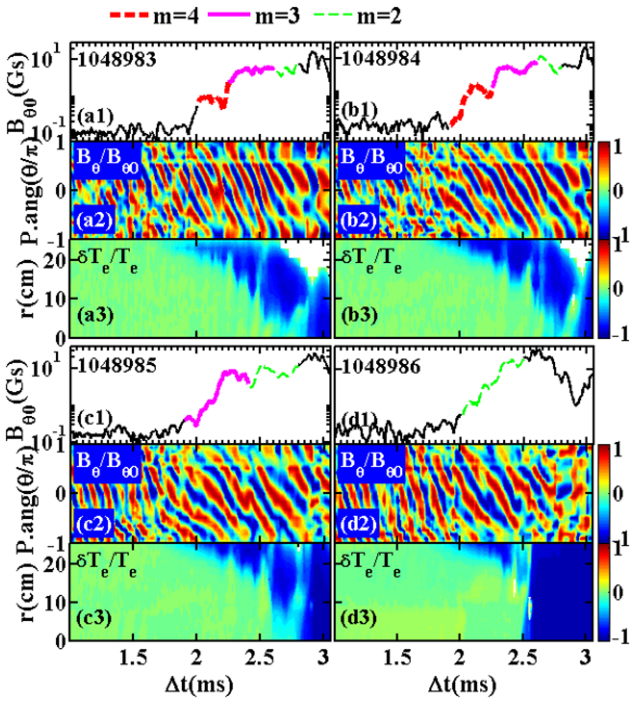

Figure 4. Time evolution of MHD instability and TQ with (*a*) $q_a = 6.3$, (*b*) $q_a = 5.5$, (*c*) $q_a = 4.5$, and (*d*) $q_a = 3.4$ for shots 1048983, 1048984, 1048985, and 1048986, respectively. Time traces of (*a*1)–(*d*1) are the magnetic perturbation amplitudes; (*a*2)–(*d*2) are the normalized poloidal magnetic perturbations: (*a*3)–(*d*3) are $\delta T_e/T_e$ from ECE signals. The times on the figure refer to the beginning time of MGI. The red, magenta, and green marks in (*a*1)–(*d*1) indicate poloidal mode. The white area in (*a*3) and (*b*3) are invalid because the optical thickness condition for ECE measurement is not satisfied.

the reason why only low m mode is observed at high density discharges. The edge safety factor limits the maximum value of m, and m decreases as the electron density increases. The poloidal mode number of the initial MHD mode triggered by MGI also decreases when more argon atoms are injected into plasma. There is no evidence for the existence of a $m/n = 6/1$ mode. Even if the 6/1 mode exists, it should be too weak to be distinguished by the Mirnov probes.

Moreover, the quantity of injected impurities increased by turning up the voltage of MGI, but the gas jet speed in vacuum increases [26]. Hence there are two variables here that may have an impact on the rate of MGI cooling the plasma, and these two are not independent.

In figure 8(*a*) the radial motion of the cooling front is shown as a function of time. The number of argon atoms of the four shots in figure 8 spans approximately two orders of magnitude. The time delay between the edge and central electron temperature collapse decreases with the increasing number of argon atoms injected, although the time when the edge of plasma starts cooling is a little different. The magnetic perturbation amplitude is the same after the cooling front reaches the core, as shown in figure 8(*a*).

Early experiments showed that the $m/n = 2/1$ tearing mode cooled down the plasma from edge towards core very quickly [34, 35]. To explore the effect of the 2/1 tearing mode, discharges with $q_a = 2.8$, central line-averaged electron density

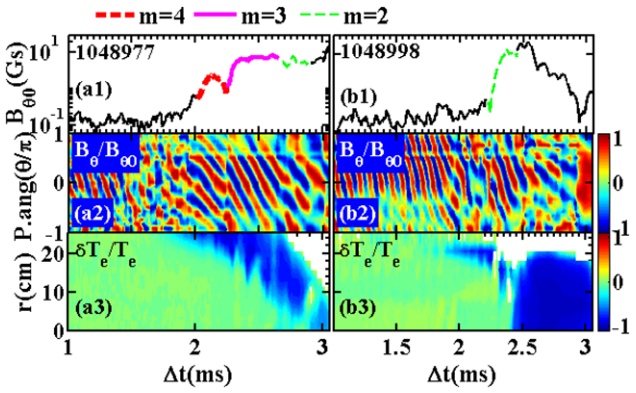

Figure 5. Poloidal magnetic perturbation and TQ with (*a*) $n_e = 1.3 \times 10^{19}$ m^{-3} and (*b*) $n_e = 2.8 \times 10^{19}$ m^{-3} for shots 1048977 and 1048998, respectively. The edge safety factors are 5.5 for both cases. The times on the figure refer to the beginning time of MGI. The white area in (*a*3) and (*b*3) are invalid because the optical thickness condition for ECE measurement is not satisfied.

about 1.2×10^{19} m^{-3} and different argon injection amounts were carried out. Figure 9 displays four shots, where the number of injected argon atoms is 2.5×10^{19}, 1.7×10^{21}, 2.5×10^{18}, 1×10^{21}, respectively. In figures 9(*a*) and (*b*) there is no big island before MGI triggering. The opposite situation is shown in figures 9(*c*) and (*d*), where a big 2/1 island is present before MGI triggering. It is clear that with such a wide range of injection, the influence of the 2/1 mode on cooling process is similar. The phase difference between ECE signals and one channel Mirnov signal in figures 9(*c*3) and (*d*3) show that the MHD activity before MGI triggering is a tearing mode according to the phase inversion. That phase inversion quickly changes after MGI triggering because of the fast cooling from edge to core. When there is no big island before MGI, the cooling process still lasts ~1.4 ms even with large scale argon injection. The cooling from edge to core of the two shots with a pre-existing 2/1 island in figure 9 occurs at the same time. A little difference exists in the time when the edge electron temperature starts collapsing, and this might be due to the change in gas injection velocity when the MGI high voltage is changed [26].

2.3. Time evolution of plasma performance after massive argon gas injected by SMBI

In subsection 2.2, it has been shown that disruptions triggered by MGI with argon injection have multiple MHD modes and a two-stage cooling process. In order to study the cooling process and associated evolution of MHD activities in more detail, SMBI (Supersonic Molecular Beam Injection) with lower gas injection rate was applied to trigger disruptions. SMBI can inject moderate argon number (injected argon number of SMBI is a function of the product of gas pressure in the valve and pulse duration) to trigger a disruption with longer duration. The SMBI argon penetration process before TQ onset is much slower than MGI.

In figure 10 there are three shots with different pulse length of SMBI, which means different amounts of impurity have been injected into vacuum vessel. The cooling from the edge

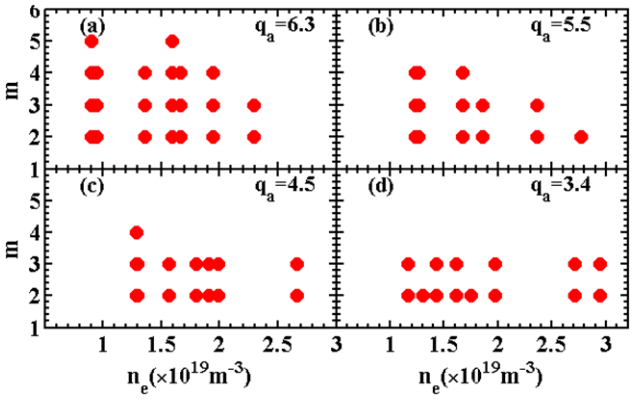

Figure 6. Dependence of poloidal mode number m on the edge safety factor and central line-average electron density. The number of argon atoms injected are about 2.1×10^{19} for all cases. Shots in each subplot have the same edge safety factor with (*a*) $q_a = 6.3$, (*b*) $q_a = 5.5$, (*c*) $q_a = 4.5$ and (*d*) $q_a = 3.4$.

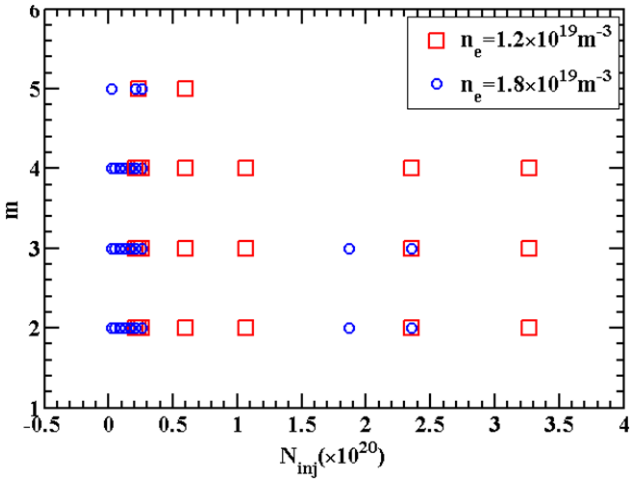

Figure 7. Dependence of poloidal mode number on the amount of Ar injected. Red squares and blue circles represent line-averaged electron densities of 1.2×10^{19} m^{-3} and 1.8×10^{19} m^{-3}, respectfully. The injected atoms are all above 10^{19}.

at $r = 20$ cm starts at about 1.8 ms after the SMBI is triggered, but the start of core plasma cooling is about 4 ms after SMBI is triggered. The core of plasma has two cooling processes, which can be seen from soft x-ray emission and ECE in the core of plasma (first at 4 ms and next at about 6–7 ms). The time duration of cooling from edge to core with impurity injected by SMBI under these settings is slower than MGI. In addition, when the pulse length of SMBI is longer than 3 ms, there is no evidence of a different cooling process, so 2 ms as the pulse length of SMBI was set in subsequent experiments.

The MHD activities of the discharges in figure 10 are very different from that triggered by MGI. The magnetic perturbations are decomposed using the equation $B_\theta = \sum_i A_i \times \sin(m_i\theta + \varphi + \Delta\Phi_i)$, where m is the poloidal mode number, θ and φ are the poloidal and toroidal angle, $\Delta\Phi_i$ is the phase of each modes, and A is the amplitude of the corresponding poloidal mode. In figure 11(*a*), the first mode is $m = 4$, then it quickly changes to $m = 3$ at ~3 ms. After 4 ms, the amplitudes of $m = 3$ and $m = 2$ modes are similar. The fast transition from $m = 4$ to $m = 3$ is consistent

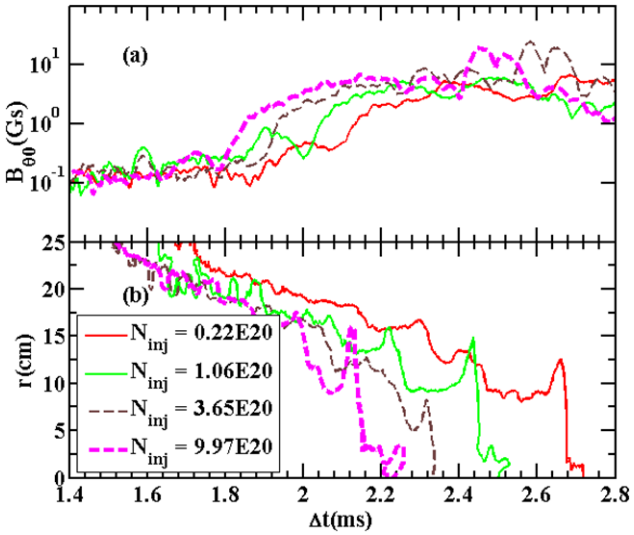

Figure 8. Dependence of magnetic perturbation and plasma cooling process on the amount of Ar injection. The different line styles represent different quantities of argon gas injection. The edge safety factors are 6.4 and the central line-average electron density are 1.5×10^{19} m^{-3}. Lines in (a) are the time trace of magnetic perturbation amplitudes. Lines in (*b*) are obtained from corresponding $\delta T_e/T_e$ contour plots, similar to that shown in figure 5, such that these lines have the same constant value of $\delta T_e/T_e$ in the coordinates $(\Delta t - r)$, showing the time evolution of the same $\delta T_e/T_e$ along the minor radius. The times on the figure refer to the beginning time of MGI.

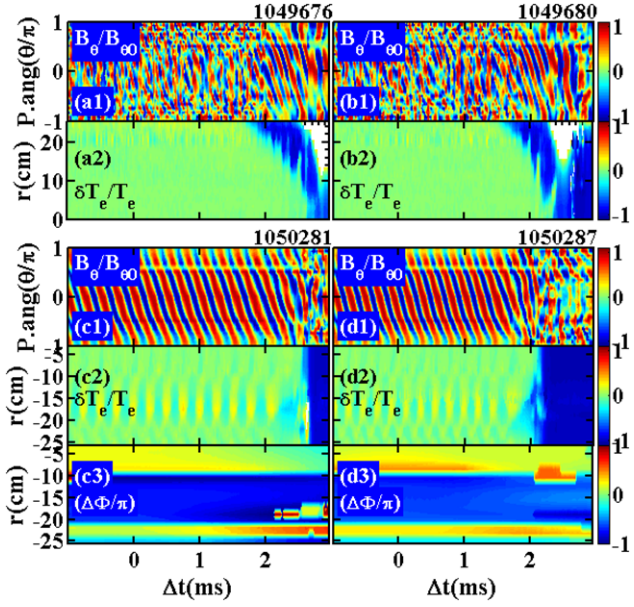

Figure 9. Figures (*a*) and (*b*) are the time evolution of MHD instability and TQ when there is no big island before MGI triggering. Figures (*c*) and (*d*) are for the cases that there is a strong 2/1 mode before MGI triggering. Figures (*c*3) and (*d*3) are the phase difference between ECE signals and one channel Mirnov signal. The number of argon atoms is (*a*) 2.5×10^{19}, (*b*) 1.7×10^{21}, (*c*) 2.5×10^{18}, (*d*) 1×10^{21}. The times on the figure refer to the beginning time of MGI. Minus radii are in the high field side. White area in (*a*2) and (*b*2) are invalid because the optical thickness condition for ECE measurement is not satisfied.

with the high speed of gas jet by SMBI (about 700 m s^{-1}). The injected argon atoms per ms by SMBI is smaller than that by MGI in these experiments. And the cooling of plasma by

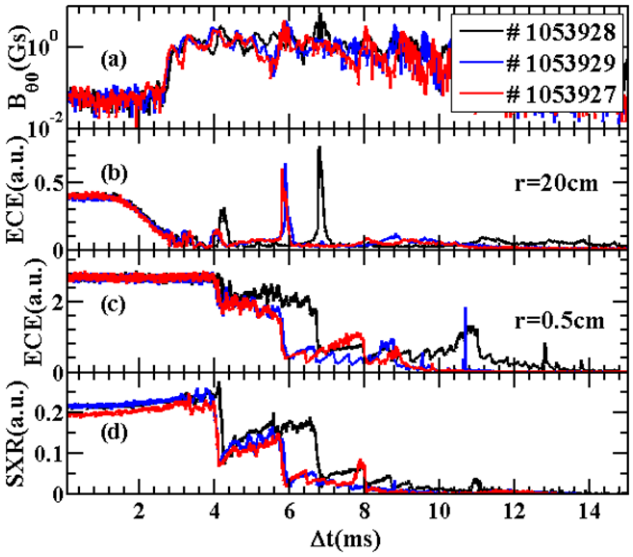

Figure 10. Three shots of different pulse length of SMBI with $q_a = 6.2$, $n_e = 1.2 \times 10^{19}$ m^{-3}, $B_T = 2.1$ T. The pulse length of SMBI in shot 1053928, 1053929 and 1053927 is 2 ms, 2.5 ms, and 3 ms, respectfully. The gas pressure of the SMBI is about 1.32–1.45 MPa. Signals from top to bottom are (*a*) amplitude of magnetic perturbation, (*b*) ECE signals at $r = 20$ cm, (*c*) ECE signals at $r = 0.5$ cm and (*d*) soft x-ray emission in the core. The times on the figure refer to the beginning time of SMBI.

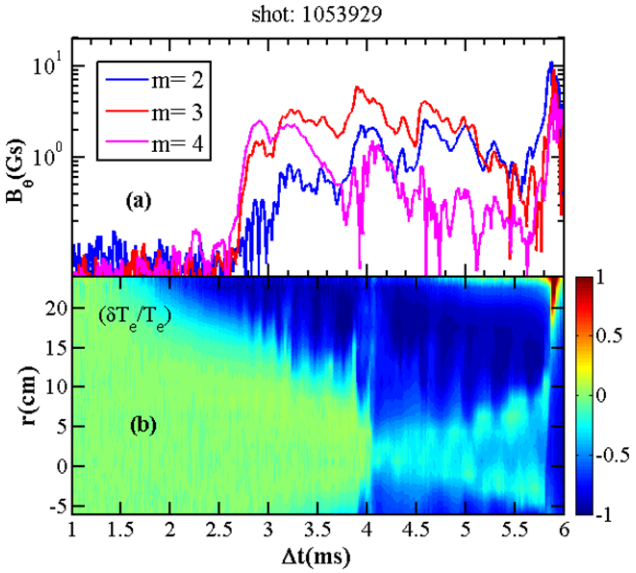

Figure 11. (*a*) Time evolution of amplitudes of $m = 4$, 3 and 2. (*b*) Time evolution of cooling process.

impurity radiation is weaker than MGI experiments, leading to smaller amplitude of MHD activities triggered by SMBI. Before a totally TQ, there is a series of partial disruption and temperature recovery as shown in figure 11(*b*).

To understand why the electron temperature has a recovery in the core, 4 discharges with different edge safety factors of 6.2, 5.4, 4.3, 3.4 are shown in figure 12. The gas pressures in the valve and pulse length of SMBI are almost the same.

The relative change of electron temperature profile in figure 12(*a*) consists of four phases: from 1.5 ms to about 4 ms after SMBI was triggered (from arrow 1 to arrow 2),

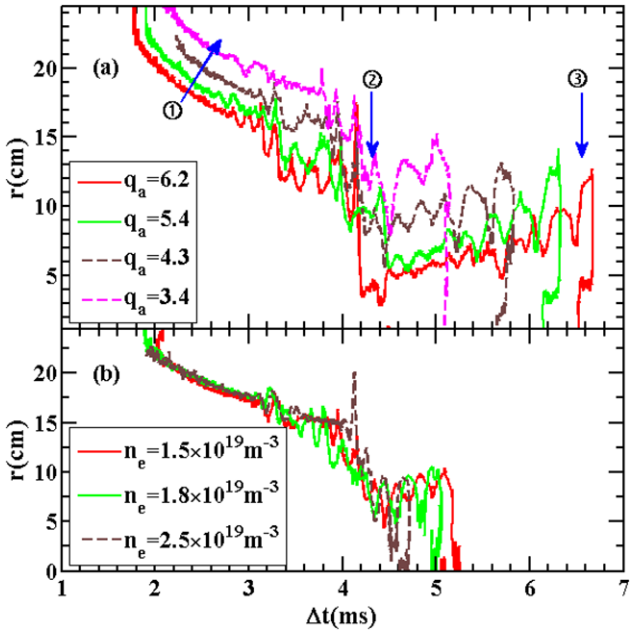

Figure 12. (*a*) Relationship between edge safety factor and electron temperature recovery. $n_e = 1.2 \times 10^{19}$ m^{-3}, $B_T = 2.1$ T for each shot here. (*b*) Relationship between electron density and electron temperature recovery. $B_T = 2.1$ T, $q_a = 4.3$ for each shot here. The gas pressure of SMBI is about 1.37–1.45 MPa. The SMBI pulse length is 2 ms for all of the shots above. Lines in (*a*) and (*b*) are obtained from corresponding $\delta T_e/T_e$ contour plots such that these lines have the same constant value of $\delta T_e/T_e$ (-0.3 in (*a*) and -0.2 in (*b*)) in the coordinates $(\Delta t - r)$, showing the time evolution of the same $\delta T_e/T_e$ along the minor radius. The times on the figure refer to the beginning time of SMBI.

the cooling front transfers linearly from edge towards core. Slightly later a fast cooling from $r \sim 14$ cm to $r \sim 8$ cm happens (near arrow 2), and then the core electron temperature falls and electron temperature of the adjacent plasma rises. The cooling front seems to propagate backward (from arrow 2 to arrow 3), and ends with an instant cooling from $r \sim 15$ cm to $r \sim 0$ cm nearly arrow 3.

As mentioned before, J-TEXT is an Ohmic-heating device, so that the change of plasma current also affect the electron temperature. In order to eliminate the effects of electron temperature, several shots with the same plasma current but different electron densities were made. In figure 12(*b*), three shots are shown with edge safety factors equal to 4.3, and electron density changes from 1.5×10^{19} m^{-3} to 2.5×10^{19} m^{-3}. The cooling process seems to have little change except for the starting time of second cooling. In figure 12(*b*) the time duration from electron temperature recovery (at about 4 ms) to the overall quench (at about 5 ms) resembles the previous results that high electron density has a sudden overall decline.

Corresponding to figure 12(*a*), the perturbation amplitudes of $m = 2$ and $m = 3$ modes shown in figure 13 reveal the evolution of poloidal modes before and after the electron temperature recovery. In shots with $q_a = 6.2$ and $q_a = 5.4$, the measured magnitude of $m = 3$ modes are larger than $m = 2$ modes at about 4 ms after SMBI is triggered. After 5 ms, the measured magnitudes of $m = 2$ modes and $m = 3$ modes are approximately equal. Considering that $q = 2$ is closer to

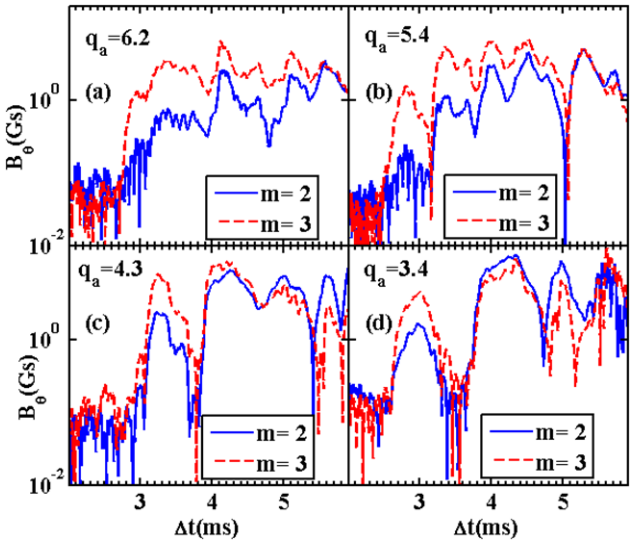

Figure 13. MHD mode amplitude of $m = 2$ and $m = 3$ after the SMBI is triggered. (a), (b), (c) and (d) correspond to shots with $q_a = 6.2$, 5.4, 4.3 and 3.4. Shots presented here are the same as those in figure 12(*a*). The times on the figure refer to the beginning time of SMBI.

Mirnov arrays than $q = 3$ surface, the dominant mode is $m = 2$ after 5 ms, implying the change of the dominant mode in the plasma. In other words, the magnitude of the $m = 2$ mode is stronger compared with the $m = 3$ mode after recovery occurs. The amplitude of the perturbation reaches its maximum value before the sudden quench. Other two cases also indicate that the $m = 2$ mode becomes stronger in a later time.

3. Discussion and summary

In summary, the MHD modes and cooling processes during disruption triggered by MGI and SMBI have been studied in J-TEXT. The behavior of MHD activities at the time of the pre-TQ and the TQ onset was described in detail. It was found that a massive number of argon atoms injected to plasma initiates MHD activities. The data presented here give a detailed description of MHD mode evolution and cooling process during the disruption triggered by a massive argon gas injection. After the argon atoms are injected, a high-m MHD mode is initiated. The poloidal mode number of this mode depends on edge safety factor, line-averaged electron density, and quantity of gas injection. The edge safety factor limits the maximum value of m. Under lower electron density or a smaller quantity of impurity injection, the MHD modes having m values closer to the edge safety factor are destabilized. As the impurity cools the plasma deeper, the MHD mode changes to a lower-m mode. When the impurity injection destabilizes a 2/1 tearing mode or there is a 2/1 mode before the MGI is triggered, cooling from edge to core is very fast. In addition, we found the plasma cooling by impurity injection can be divided into two parts: diffusive cooling and oscillating cooling. The oscillating period of cooling front is similar to the MHD rotating period, which suggests that cooling may be modulated by MHD activity.

Acknowledgments

The authors are very grateful for the help of J-TEXT team and the modifications of Alan Coulter England. This work was supported by the National Magnetic Confinement Fusion Science Program (Nos. 2015GB111001, 2015GB111002 and 2015GB104000) and by the National Natural Science Foundation of China (Nos. 11505069, 11775089, 71762031 and 11575068).

ORCID iDs

Z.Y. Chen https://orcid.org/0000-0002-8934-0364
Z.H. Jiang https://orcid.org/0000-0002-4971-080X

References

[1] Riccardo V. and JET EFDA contributors 2003 Disruptions and disruption mitigation *Plasma Phys. Control. Fusion* **45** A269
[2] Schuller F.C. 1995 Disruptions in tokamaks *Plasma Phys. Control. Fusion* **37** A135
[3] Chen Z.Y. *et al* 2016 The behavior of runaway current in massive gas injection fast shutdown plasmas in J-TEXT *Nucl. Fusion* **56** 112013
[4] Hollmann E.M. *et al* 2015 Status of research toward the ITER disruption mitigation system *Phys. Plasmas* **22** 021802
[5] Hollmann E.M. *et al* 2008 Measurements of injected impurity assimilation during massive gas injection experiments in DIII-D *Nucl. Fusion* **48** 115007
[6] Hollmann E.M. *et al* 2005 Measurements of impurity and heat dynamics during noble gas jet-initiated fast plasma shutdown for disruption mitigation in DIII-D *Nucl. Fusion* **45** 1046–55
[7] Taylor P.L. *et al* 1999 Disruption mitigation studies in DIII-D *Phys. Plasmas* **6** 1872–9
[8] Pautasso G. *et al* 2007 Plasma shut-down with fast impurity puff on ASDEX Upgrade *Nucl. Fusion* **47** 900–13
[9] Lehnen M. *et al* 2011 Disruption mitigation by massive gas injection in JET *Nucl. Fusion* **51** 123010
[10] Thornton A.J. *et al* 2012 Characterization of disruption mitigation via massive gas injection on MAST *Plasma Phys. Control. Fusion* **54** 125007
[11] Whyte D.G. *et al* 2003 Disruption mitigation with high-pressure noble gas injection *J. Nucl. Mater.* **313** 1239–46
[12] Izzo V.A. *et al* 2008 Magnetohydrodynamic simulations of massive gas injection into Alcator C-Mod and DIII-D plasmas *Phys. Plasmas* **15** 056109
[13] Hollmann E.M. *et al* 2007 Observation of q-profile dependence in noble gas injection radiative shutdown times in DIII-D *Phys. Plasmas* **14** 012502
[14] Hopcraft K.I. *et al* 1988 Comparison of tokamak disruption simulations *Nucl. Fusion* **28** 1265
[15] Reinke M.L. *et al* 2008 Toroidally resolved radiation dynamics during a gas jet mitigated disruption on Alcator C-Mod *Nucl. Fusion* **48** 125004
[16] Izzo V.A. 2006 A numerical investigation of the effects of impurity penetration depth on disruption mitigation by massive high-pressure gas jet *Nucl. Fusion* **46** 541–7
[17] Izzo V.A. 2013 Impurity mixing and radiation asymmetry in massive gas injection simulations of DIII-D *Phys. Plasmas* **20** 056107

[18] Fil A. *et al* 2015 Three-dimensional non-linear magnetohydrodynamic modeling of massive gas injection triggered disruptions in JET *Phys. Plasmas* **22** 062509
[19] Nardon E. *et al* 2017 Progress in understanding disruptions triggered by massive gas injection via 3D non-linear MHD modelling with JOREK *Plasma Phys. Control. Fusion* **59** 014006
[20] Zhuang G. *et al* 2011 The reconstruction and research progress of the TEXT-U tokamak in China *Nucl. Fusion* **51** 094020
[21] Zhuang G. *et al* 2015 Overview of the recent research on the J-TEXT tokamak *Nucl. Fusion* **55** 104003
[22] Huang M. *et al* 2016 The operation region and MHD modes on the J-TEXT tokamak *Plasma Phys. Control. Fusion* **58** 125002
[23] Guo D. *et al* 2017 Upgrade of the Mirnov probe arrays on the J-TEXT tokamak *Rev. Sci. Instrum.* **88** 123502
[24] Yang Z.J. *et al* 2012 A 16-channel heterodyne electron cyclotron emission radiometer on J-TEXT *Rev. Sci. Instrum.* **83** 10E313
[25] Yang Z.J. *et al* 2016 Electron cyclotron emission radiometer upgrade on the J-TEXT tokamak *Rev. Sci. Instrum.* **87** 11E112
[26] Tang Y. *et al* 2015 Observation of the penetration of massive gas jet by fast frame camera on J-TEXT *Phys. Lett.* A **379** 1043–7
[27] Luo Y.H. *et al* 2014 Designing of the massive gas injection valve for the joint Texas experimental tokamak *Rev. Sci. Instrum.* **85** 083504
[28] Xiao J.S. *et al* 2015 A supersonic molecular beam injection system on the J-TEXT tokamak *J. Fusion Energy* **34** 1020–6
[29] Wesson J. 2004 *Tokamaks* (Cambridge, MA: Oxford University Press)
[30] Gibson A. 1976 Radiation limits to tokamak operation *Nucl. Fusion* **16** 546
[31] Connor J.W. and You S. 2002 On the density limit in tokamaks *Plasma Phys. Control. Fusion* **44** 121
[32] Shi P. *et al* 2017 First time observation of local current shrinkage during the MARFE behavior on the J-TEXT tokamak *Nucl. Fusion* **57** 116052
[33] Yan W. *et al* 2016 Measurement of the electron and ion temperatures by the x-ray imaging crystal spectrometer on joint Texas experimental tokamak *Rev. Sci. Instrum.* **87** 11E318
[34] Thornton A.J. *et al* 2012 Plasma profile evolution during disruption mitigation via massive gas injection on MAST *Nucl. Fusion* **52** 063018
[35] Hender T.C. *et al* 2007 Chapter 3: MHD stability, operational limits and disruptions *Nucl. Fusion* **47** S128